Int. J. Electrochem. Sci., 15 **(2020)** 10971 – 10978, doi: 10.20964/2020.11.52

International Journal of
ELECTROCHEMICAL
SCIENCE
www.electrochemsci.org

Short Communication

Al Thin Films Electrodeposited on Copper in an Aqueous Solution

M. Saitou

University of the Ryukyus, Department of Mechanical Systems Engineering, 1 Senbaru Nishihara-cho Okinawa, 903-0213, Japan.
E-mail: saitou@tec.u-ryukyu.ac.jp

Received: 14 July 2020 / *Accepted:* 9 September 2020 / *Published:* 30 September 2020

Electrodeposits formed from an aqueous solution by rectangular pulse voltages over a megahertz frequency range were investigated through scanning electron microscopy-energy dispersive X-ray (SEM-EDX) microanalysis and X-ray diffraction (XRD). The SEM-EDX analysis demonstrated that the electrodeposits comprised Al. The current efficiency increased with the cathode potential and tended to become constant, which is in accordance with the phenomenological theory of electrodeposition. The oscillatory change in the current efficiency occurred at resonant frequencies when the cathode potential was equal to the Al^{3+} potential barrier. The maximum current efficiency was 2.6 % at the resonant frequencies. XRD analysis revealed that the Al thin films had amorphous structures.

Keywords: Al thin film; aqueous solution; potential barrier; cathode potential; amorphous structure

1. INTRODUCTION

It has been reported that the electrodeposition of an Al thin film from an aqueous solution [1–3] is very difficult because of the high negative standard electrode potential of Al^{3+}/Al (-1.662 V) [4] and hydrogen evolution on the cathode. Hence, Al electrodeposition has been performed using organic solvents [5–8] or inorganic molten salts [9–11]. However, the standard electrode potential that accounts for thermal equilibrium cannot always represent electrodeposition as a non-equilibrium phenomenon. If a less notable element in the standard electrode potentials table is preferentially deposited, it is termed ‘anomalous co-deposition’ [12] within a thermal equilibrium framework.

Recently, a phenomenological theory of electrodeposition based on the energy band diagram [13] has been proposed. Theoretically, the probability of electrodeposition is determined by the cathode potential, potential barrier, and resonant frequencies. Hence, Al^{3+} ions have a probability of atomisation only if Al^{3+} ions near the electric double layer on a cathode have energy levels to which electrons at the Fermi state in the cathode can transit. This study demonstrates that Al thin films were electrodeposited

from an aqueous solution and followed the phenomenological theory.

Amorphous Al and Al alloys, called metallic glasses, have attracted research interest owing to their high tensile yield stress (≥ 1GPa) [14–16]. They do not lose metallic properties and have good electrical and thermal conductivities as well as corrosion resistance. Amorphous Al materials are often produced by the extremely rapid cooling of Al liquid. Electrodeposition is a low-cost and easy method for fabricating amorphous iron group metals such as Fe [17], Ni-P [18], and Co-Mo [19]. This study reveals that Al thin films have amorphous structures.

This study aims to demonstrate that Al thin films were electrodeposited from an aqueous solution, followed the phenomenological theory, and had amorphous structures.

2. EXPERIMENTAL SETUP

An aqueous solution containing $AlSO_4 \cdot 16H_2O$ (0.4 mol L^{-1}) and $KNaC_4H_4O_6 \cdot 4H_2O$ (0.4 mol L^{-1}) was prepared. A 30 ×10 × 0.2 mm^3 copper (Cu) plate (99.95 wt% Cu) and 50 × 40 mm^2 carbon (C) plate were used as the cathode and anode. One side of the Cu plate was electrically insulated; electrodeposition was performed on the other side. The two electrodes were placed parallel to each other in an electrochemical cell filled with an aqueous solution. The solution was kept at 300 K during electrodeposition.

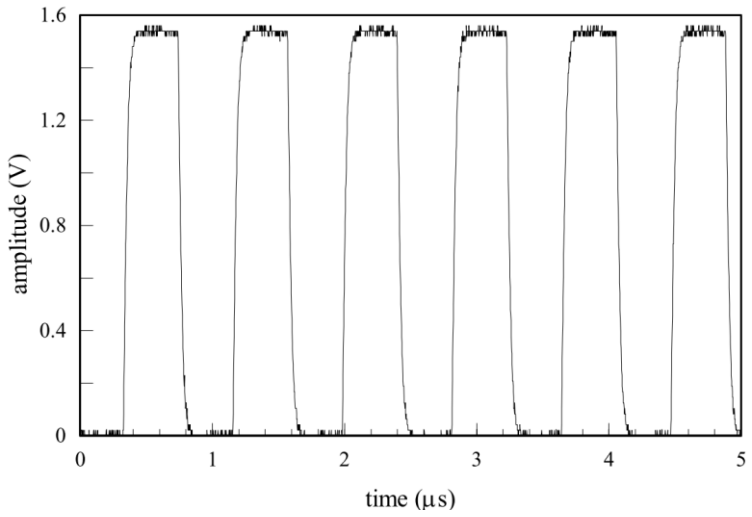

Figure 1. Voltage drops measured across the 22 Ω resistor when a rectangular pulse voltage of 7 V amplitude and 1.2 MHz frequency was applied to the cell.

Al thin films were electrodeposited on the Cu plates immersed to a depth of 15 mm in the solution. The area of the C plate was approximately 27 times greater than that of the immersed Cu plate; hence, the impedance of the electric double layer in series with the C electrode in the solution can be neglected. The impedance between the cathode and anode can also be ignored because of the concentrated aqueous solution.

A rectangular pulse voltage in the frequency range of 0.5–1.3 MHz was supplied to the cell by a function generator. A 22 Ω metal film resistor was connected in series with the cell to determine the cathode potential and current flowing to the cell. The voltage drop across the metal film resistor was measured using a digital storage oscilloscope.

Figure 1 shows a typical rectangular pulse voltage measured across the metal film resistor when a rectangular pulse voltage of 7 V amplitude and 1.2 MHz frequency was applied to the cell. The cathode potential was 5.46 V by calculating the amplitude (7 V) minus the pulse voltage (1.54 V).

The electrodeposits on the Cu plate were rinsed with distilled water and dried in a vacuum chamber after electrodeposition. The electrodeposits were weighed to a precision of 0.1 mg with an electric balance to calculate the current efficiency defined by the ratio between the electrodeposit mass and Al mass expected by the current passing through the cell.

Electrodeposits on the Cu plate were investigated using scanning electron microscope-energy dispersive X-ray (SEM-EDX) microanalysis (Hitachi TM3030). The crystallographic structure of electrodeposits was determined through X-ray diffraction (XRD) (Rigaku Ultima) with CuKα radiation using carbon monochromators.

3. RESULTS AND DISCUSSION

3.1 Determination of the electrodeposit composition

Figure 2 shows the SEM images of the electrodeposits and their composition determined by SEM-EDX analysis.

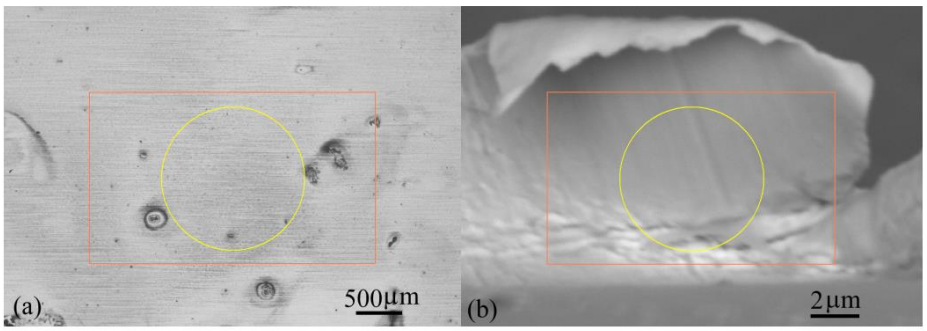

element	[at%]
copper	92.6
aluminum	7.4

element	[at%]
copper	61.6
aluminum	38.4

Figure 2. SEM images and Al contents of electrodeposits formed with a frequency of 1.2 MHz. (a) Thin film electrodeposited on a 15 ×10 mm^2 Cu surface at 6.41 V cathode potential. The Al composition was measured within a circle of 1500 µm diameter. (b) Detached thin film electrodeposited on a 15 × 0.2 mm^2 Cu end surface at 3 V cathode potential. The Al composition was measured within a circle of 6 µm diameter.

The thin film in Fig. 2 (a) was formed on a 15 × 10 mm^2 Cu surface at 6.41 V cathode potential and 1.2 MHz frequency. EDX analysis demonstrated that the thin film on the Cu surface comprised Al. The mean Al composition of the thin film within a circle of 1500 μm diameter was found to be 7.4 at% from the characteristic X-ray of the Cu plate.

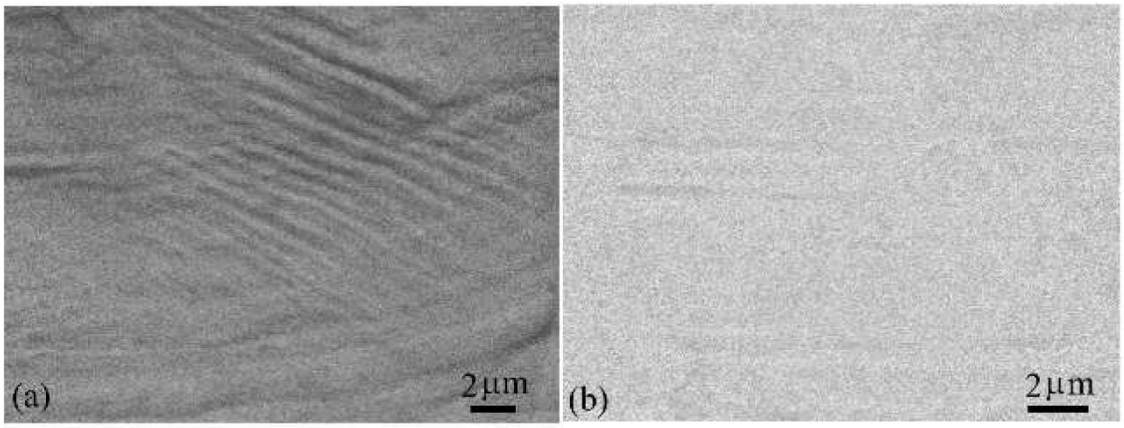

Figure 3. SEM images of Al thin films electrodeposited (a) at 2.68 V cathode potential and 1.25 MHz frequency, and (b) at 6.61 V cathode potential and 1.2 MHz frequency.

Figure 2 (b) shows a thin film separated from a 10 × 0.2 mm^2 Cu end surface. The Al composition of the thin film within a circle of 6 μm diameter was much higher than that in Fig. 2 (a) because the thin film was separated from the Cu end surface. Therefore, Al was identified as the element of the electrodeposits.

Figures 3 (a) and (b) show the SEM images of Al thin films electrodeposited on Cu plates at 2.68 V cathode potential and 1.25 MHz frequency, and at 6.61 V cathode potential and 1.2 MHz frequency, respectively. The surface morphology in Fig. 3 (a) appears to comprise steps, terraces, and kinks, which are formed by the layer by layer growth according to the Burton-Cabrera-Frank surface growth mechanism [20]. The step distance seems to be approximately constant. The surface might be smooth at an atomic level. Figure 3 (b) also demonstrates that the surface was uniformly smooth.

3.2 Current efficiency predicted by the phenomenological theory

Figure 4 shows a schematic diagram of the current efficiency derived from the phenomenological theory on electrodeposition [13]. This theory, which is based on the band energy, predicts the current efficiency of Al thin films as follows: (1) when the cathode potential (V_c) increases and reaches the Al^{3+} potential barrier (V_{bAl}^{3+}) the number of electrons that can pass through the electric double layer from the Fermi level in the cathode to the upper state of Al^{3+} ions increases owing to the tunnelling effect described by the Fowler–Nordheim equation [21].

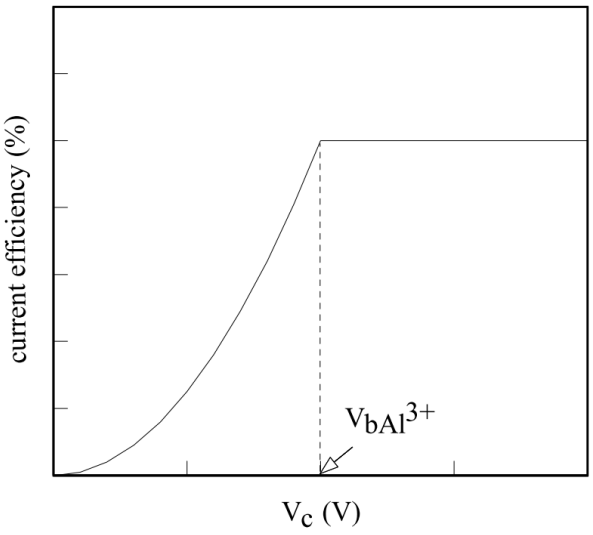

Figure 4. Schematic diagram of the current efficiency based on the phenomenological theory.

An increase in the probability of the transition from an Al^{3+} ion to an Al atom on the cathode increases the current efficiency. (2) when $V_c = V_{bAl}^{3+}$, the current efficiency significantly changes at resonant frequencies [22]. (3) when $V_c > V_{bAl}^{3+}$, the current efficiency tends to become constant because the electric double layer only acts as an impedance on electrons passing through it.

3.3 Current efficiency dependent on the cathode potential

Figure 5 shows the dependence of the current efficiency on the cathode potential. According to the phenomenological theory, the current efficiency increases with V_c and tends to become constant. When $V_c = V_{bAl}^{3+}$, oscillatory changes occur in the current efficiency at resonant frequencies. Figure 5 demonstrates that the current efficiency increases with the cathode potential as shown in Fig. 4. The potential barrier of Al^{3+} was determined to be 4.28 V from the intersection point of the current efficiency curve, which increases with the cathode potential, and the current efficiency line displaying a constant value.

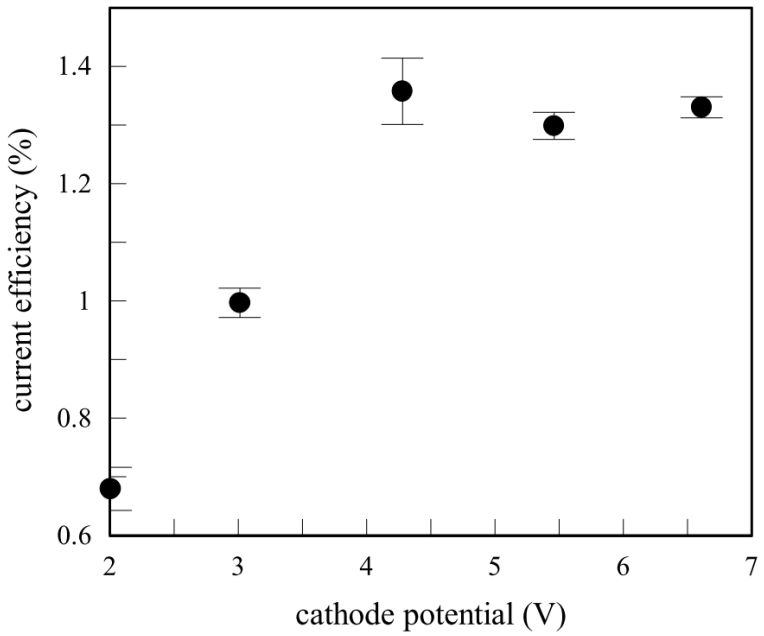

Figure 5. Dependence of the current efficiency of the electrodeposited Al thin films on the cathode potential at 1.2 MHz frequency.

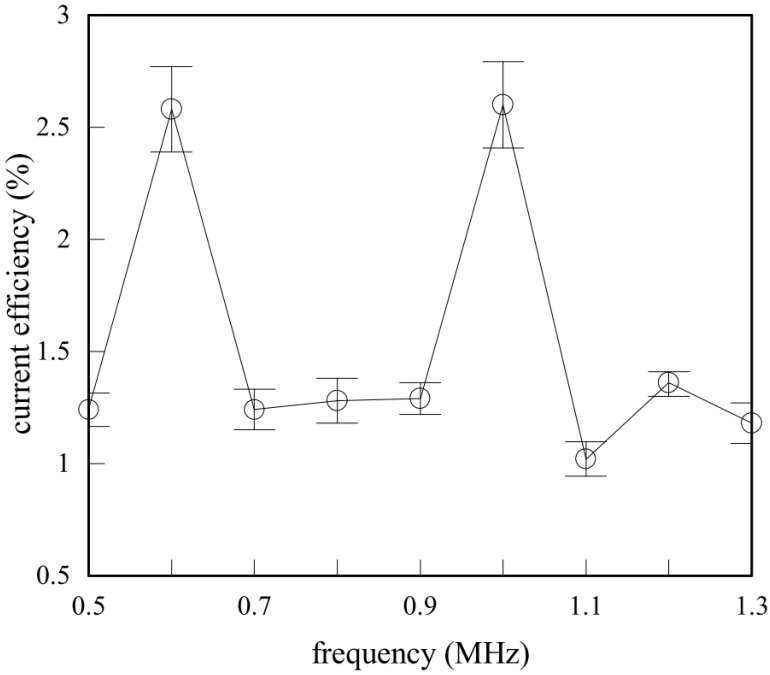

Figure 6. Dependence of the current efficiency of the electrodeposited Al thin films on the frequency at 4.28 V cathode potential.

Figure 6 shows the oscillation of the Al current efficiency at the resonant frequencies. Al thin films were formed at a cathode potential of 4.28 V and frequency in the range of 0.5–1.3 MHz. The current efficiencies had local maximum values at 0.6 and 1.0 MHz; the frequencies were resonant. The

resonant frequency spacing was 0.4 MHz. The maximum current efficiency level was low (2.6 at%). This suggests that the number of Al^{3+} ions near the electric double layer was low, and some currents passed as non-faradic currents and were consumed by hydrogen evolution.

3.4 Crystalline structure of Al thin films

Figure 7 shows an XRD pattern of a 2.0 μm-thick Al thin film electrodeposited at 6.61 V cathode potential and 1.2 MHz frequency. No diffraction peaks were observed for the Al thin film. Hence, it had an amorphous structure.

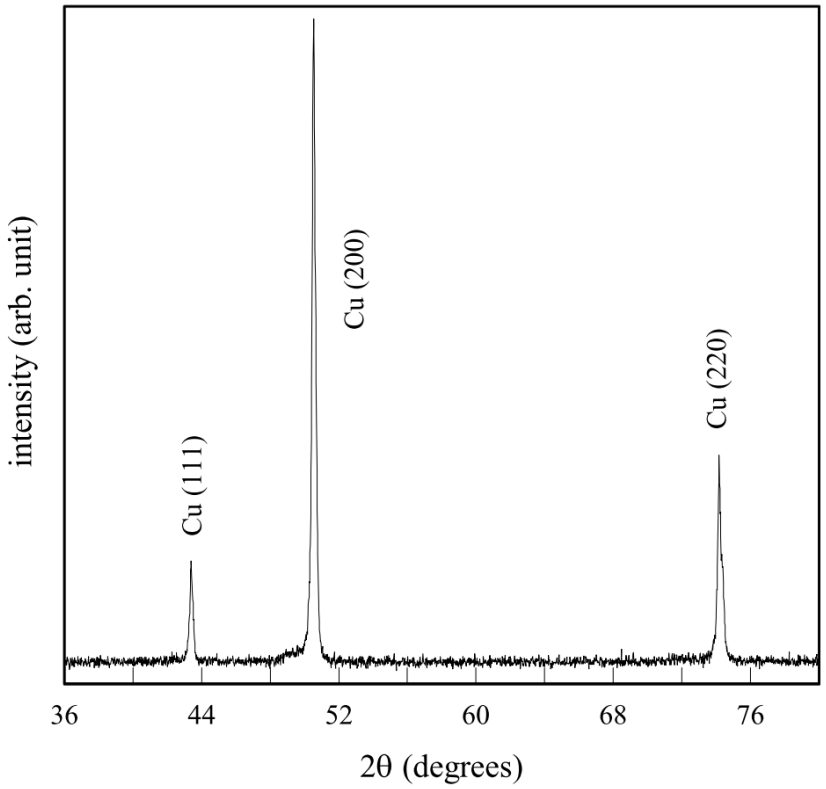

Figure 7. XRD pattern of a 2.0 μm-thick Al thin film electrodeposited at 6.61 V cathode potential and 1.2 MHz frequency.

4. CONCLUSIONS

Electrodeposits formed from an aqueous solution comprising $AlSO_4 \cdot 16H_2O$ and $KNaC_4H_4O_6 \cdot 4H_2O$ were identified as Al using SEM-EDX analysis. The current efficiency of the Al thin films increased with cathode potential and tended to become constant. The oscillatory change in the current efficient occurred at 0.6 and 1.0 MHz resonant frequencies when the cathode potential was equal to the Al^{3+} potential barrier of 4.28 V. These results were consistent with the phenomenological theory

of electrodeposition. The maximum current efficiency was 2.6 %. The XRD analysis revealed that the Al thin films had amorphous structures.

References

1. M. Galindo, P. Sebastián, P. Cojocaru, and E. Gómez, *J. Electroanal. Chem.*, 41 (2018) 41.
2. Y. Hou, R. Li, and J. Liang, *Appl. Surf. Sci.*, 434 (2018) 918.
3. G. Yue, S. Zhang, Y. Zhu, X, Lu, S. Li, and Z. Li, *AIChE J*., 55 (2009) 783.
4. D. R. Lide, *CRC Handbook of Chemistry and Physics*, 79th ed., New York, CRC Pr., (1998).
5. Y. Yang, S. Liu, C. Chi, J. Hao, J. Zhao, Y. Xu, and Y. Li, *J. Mater. Sci.:Mater. Electron*, 31 (2020) 9937.
6. D. Wang, X. Zhong, F. Liu, and Z. Shi, *Int. J. Electrochem. Sci.*, 14 (2019) 9489.
7. Y. Zheng, Y. Zheng, Q. Wang, Z. Wang, and C. Peng, *Int. J. Electrochem. Sci.*, 13 (2018) 10948.
8. A. Bakkar and V. Neubert, *Electrochem. Commun*., 51 (2015) 113.
9. M. Ueda, *J. Solid State Electrochem.*, 21 (2017) 641.
10. M. Li, B. Gao, W. Chen, C. Liu, Z. Wang, Z. Shi, and X. Hu, *Electrochim. Act.*, 185 (2015) 148.
11. J. Xu, J. Zhang, and Z. Shi, *High Temp. Mater. Proc.*, 32 (2012) 367.
12. S. Swathirajam, *J. Electroanal. Chem.*, 221 (1987) 211.
13. M. Saitou, *Int. J. Electrochem. Sci.*, 15 (2020) 6561.
14. J. H. Perepezko and R. J. Hebert, *JOM*, 54 (2002) 34.
15. A. L. Greer, *Nature*, 368 (1994) 688.
16. E. Fourgas and Y. Sheng, *AIP Adv.*, 10 (2020) 045319.
17. M. Saitou, *Int. J. Electrochem. Sci.*, 15 (2020) 434.
18. M. M. V. Parente, O. R. Mattos, S. L. Díaz, P. L. NETO, and F. J. F. Miranda, *J. Appl. Electrochem.*, 31 (2001) 677.
19. E. Gómez, E. Pellicer, X. Alcobé, and E. Vallés, *J. Solid State Electrochem.*, 8 (2004) 497.
20. W. K. Burton, N. Cabrera, and F. C. Frank, *Philos. Trans. R. Soc. London Ser. A*, 243 (1951) 299.
21. R. H. Fowler and L. Nordheim, *Proc. R. Soc. Ser. A*, 119 (1928) 173.
22. M. Saitou, *Int. J. Electrochem. Sci.*, 11 (2016) 5535.